ICAS-80-7.5

A RAPID METHOD FOR THE APPROXIMATE DETERMINATION OF NONLINEAR SOLUTIONS: APPLICATION TO AERODYNAMIC FLOWS

Stephen S. Stahara, James P. Elliott
Nielsen Engineering & Research, Inc.
Mountain View, California

and

John R. Spreiter
Stanford University
Stanford, California

Abstract

A method for determining highly accurate approximations to families of strongly nonlinear solutions which are either continuous or discontinuous, and which represent variations in some arbitrary parameter, is developed and evaluated. The procedure consists of defining a unit perturbation by employing two or more nonlinear solutions which differ from one another by a nominal change in some geometric or flow parameter, and then using that unit perturbation to predict a family of related nonlinear solutions over a range of parameter variation. Coordinate straining is used in determining the unit perturbation to account for the movement of discontinuities and maxima of high-gradient regions due to the perturbation. Although the procedure is generally applicable, results are presented here for nonlinear aerodynamic applications. Attention is focused in particular on transonic flows which are strongly supercritical and exhibit large surface shock movement over the parametric range studied; and on subsonic flows which display large pressure variations in the stagnation and peak suction pressure regions. Flows past both isolated airfoils and compressor cascades involving a variety of flow and geometry parameter changes are considered. Comparisons with the corresponding 'exact' nonlinear solutions indicate a remarkable accuracy and range of validity of such a procedure. Computational time is trivial.

Introduction

Given the remarkable growth in capability of advanced computational methods for the determination of a spectrum of nonlinear phenomena in such diverse disciplines as fluid dynamics, structures, and nuclear physics to name just a few - a capability which has already made many difficult calculations routine and which is certain to improve in the future - it is apparent that a need exists for complimentary methods capable of alleviating, at least in part, the usage limitations imposed on these methods by their run times. The need becomes particularly compelling when large numbers of related cases are required as in parametric or design studies. Techniques such as direct acceleration procedures provide an important means of reducing computer time by improving computational efficiency of the solution algorithm, but these and similar methods, which enhance the solution algorithm itself, represent only a partial answer. What is most desirable is a means to minimize the actual number of separate calculations required in a particular application by extending, over some parametric range, the usefulness of each individual solution determined by these computationally-expensive procedures. Two fundamental methods for accomplishing this are available: a classical approach involving posing and solving linear perturbation equations; and a direct differencing method employing two or more nonlinear base solutions. In this paper, both of these methods are discussed; and an evaluation of the latter method, based on a large number of different applications is made.

A crucial aspect of such perturbation methods is their ability to accurately treat regions where either discontinuities or high gradients exist. For the results presented here coordinate straining is introduced as a means of accounting properly for the displacement of discontinuities due to an arbitrary change in some solution parameter. This is shown to result in highly-accurate perturbation predictions in the vicinity of the discontinuity. That idea has also been extended to improve predictions in the vicinity of other high-gradient regions.

Although the procedures developed are generally applicable, the specific results reported here are for aerodynamic applications. Single-parameter and simultaneous multiple-parameter perturbation results based on transonic small-disturbance and full potential solutions are presented for nonlinear subsonic and transonic flows past both isolated airfoils and compressor cascades. In order to enable a critical evaluation of the range of validity and accuracy of the straining procedure, emphasis is placed on transonic flows which are strongly supercritical and exhibit large surface shock movement over the parametric range studied; and on subsonic flows which display large pressure variations in the stagnation and peak suction pressure regions.

Analysis

Perturbation Concept and Methods

The basic hypothesis underlying the present procedure is that a range of solutions in the vicinity of a previously-determined or base solution can be calculated to first-order accuracy in the incremental change of the varied parameter by determining a linearized unit perturbation solution Q_p defined according to the relation

$$\overbrace{Q}^{\substack{\text{Approximate solution for conditions differing from those of the base solution by an amount characterized by } \Delta}} = \overbrace{Q_o}^{\substack{\text{Base solution for some flow quantity } Q}} + \overbrace{\Delta \cdot \{Q_p\}}^{\substack{\text{Linearized perturbation solution for a unit change of } \Delta}} \qquad (1)$$

The effectiveness of such a method, of course, depends upon the ability of the relationship defined by Eq. (1) to remain accurate over a range Δ of practical significance, and the fact that the unit perturbation Q_p need be determined only once. The significance of the unit perturbation Q_p is obvious. It represents the local rate of change of the base flow solution Q_o with respect to the particular quantity, say q, perturbed; that is $Q_p = (\partial Q/\partial q)_o$.

Two generic methods exist for determining Q_p, each differing in philosophy and having its own particular strengths and weaknesses. We refer to these methods simply as the linear perturbation equation method and the direct correction method.

The linear perturbation equation method represents the classical approach for performing a perturbation analysis and proceeds by establishing and solving a linear differential equation for the perturbation. Although in the present application, we confine our interest solely to the first-order term, the complete procedure represents a rational approximation scheme capable of continuation to any order. The method proceeds by expanding the dependent variables in an ascending power series in the incremental change Δ of the varied parameter, inserting that representation into the full governing equations, and then assembling the result into a corresponding series of linear equations in ascending orders in Δ. Higher-order solutions in general depend on both base flow plus lower-order solutions. Determination of the appropriate boundary conditions is done in a similar fashion.

The power of the linear perturbation equation method is that it requires the calculation of only one nonlinear base solution. With that information, any number of individual perturbations can then be calculated, subject to the particular governing linear partial differential equations and boundary conditions which apply. The disadvantages are that each perturbation problem must be posed individually, including differential equations and boundary conditions. Furthermore, it may be necessary to simplify the govering equations and boundary conditions to a point where they can be solved rapidly relative to rerunning the base flow procedure. Moreover, the perturbation solutions themselves may be quite sensitive to the base flow solutions which usually enter into the perturbation problem through the differential equation and sometimes through the boundary conditions as well.

The fundamental limitation of the method is the restriction of the range over which the perturbation procedure remains valid to a linear one. Since this characteristic depends upon the local behavior of the base flow with respect to the varied parameter, no general statement regarding range of validity is possible. Typical behavior for a given class of flows must be ascertained by checks with the base flow procedure. Initially unknown at the outset of an application with this technique, then, are the accuracy requirements imposed on the base solution by the perturbation procedure and the range of parameter variation over which the linear assumption is valid.

For the alternative method, the perturbation solution per unit change of the varied parameter, Q_p, is determined simply by differencing two nonlinear base flow solutions removed from one another by some nominal change of a particular flow or geometrical quantity. A unit perturbation solution is then obtained by dividing that result by the change in the perturbed quantity. Related solutions are determined by multiplying the unit perturbation by the desired parameter change and adding that result to the base flow solution. This simple procedure, however, only works directly for continuous flows for which the perturbation change does not alter the solution domain. For those perturbations which change the flow domain, coordinate stretching (usually obvious) is necessary to insure proper definition of the unit perturbation solution. Similarly, for discontinuous flows, coordinate straining is necessary to account for movement of discontinuities due to the perturbation solution.

The attractiveness of the correction method is that it is not restricted to a linear variation range but rather replaces the nonlinear variation between two base solutions with a linear fit. This de-emphasizes the dependence and sensitivity inherent in the linear perturbation equation method on the local rate of change of the base flow solution with respect to the varied quantity. For many applications, particularly at transonic speeds, the flow is highly sensitive, and the linear range of parameter variation can be sufficiently small to be of no practical use. Furthermore, other than the approximation of a linear fit between two nonlinear base solutions, the direct correction method is not restricted by further approximations with respect to the governing differential equations and boundary conditions. Rather, it retains the full character of the original methods used to calculate the base flow solutions. Most importantly, no perturbation differential equations have to be posed and solved, only algebraic ones. In fact, it isn't necessary to know the exact form of the perturbation equation, only that it can be obtained by some systematic procedure and that the perturbations thus defined will behave in some 'generally appropriate' fashion so as to permit a logical perturbation analysis. For situations involving perturbations of physical parameters, such as reported here, the governing perturbation equations are usually transparent, or at least readily derivable. Finally, in applying this method it isn't necessary to work with primitive variables; rather the procedure can be applied directly to the final quantity desired.

The primary disadvantage of this method is that two base solutions are required for each parameter perturbation considered. Furthermore,

both flows must be topologically similar, i.e., discontinuities or other characteristic features must be present in both base solutions used to establish the unit perturbation.

Previous Applications

Detailed studies of the linear perturbation equation method to sensitive transonic flows, with a view toward testing the method as an effective tool for reducing computational requirements, have not been done. The primary reason is that such studies quickly become overwhelming. Each perturbation problem must be posed individually, subject to its own particular governing equations and boundary conditions; and then a separate computational code for the perturbation established. Generally, the governing equations and boundary conditions of the perturbation, even though they are linear, are more involved than those for the base solution. Additionally, the computational and convergence characteristics can pose similar or additional problems from those of the base flow procedure.

In an attempt to examine some of these problems for transonic applications in at least a preliminary fashion, an application of the linear perturbation equation method to transonic turbomachinery flows was made in reference 1. The conclusions obtained from that study were that reasonable results could be anticipated from the method for blade geometry changes, such as blade thickness and angle of attack. Less satisfactory results were obtained for perturbation changes in overall quantities, such as blade spacing and free-stream Mach number, a result that could be anticipated a priori since such perturbations alter the basic character of the flow more rapidly. The most significant conclusion of that study was the demonstration of the primary limitation of the linear perturbation equation method. That is, for sensitive flows such as occur in transonic situations, the basic linear variation assumption fundamental to the technique is sufficiently restrictive that the permissible range of parameter variation becomes so small as to be of limited practical use. Some preliminary applications of the direct correction method, however, displayed a significantly wider range of perturbation solution validity, in particular for strongly supercritical flows when coordinate straining was employed to account for shock movement.

Coordinate Straining

The concept of employing coordinate straining to remove nonuniformities from perturbation solutions of nonlinear problems is well-established and originally suggested by Lighthill[2] three decades ago. The basic idea of the technique is that a straightforward perturbation solution may possess the appropriate form, but not quite at the appropriate location. The procedure is to slightly strain the coordinates by expanding them as well as the dependent variables in an asymptotic series. It is often unnecessary to actually solve for the straining. It can generally be established by inspection. The final uniformly-valid solution is then found in implicit form, with the strained coordinate appearing as a parameter.

In the original applications of the method,[3] it was applied in the 'classical' sense; that is, series expansions of the dependent and independent variables in ascending powers in some small parameter were inserted into the full governing equation and boundary conditions, and the individual terms of the series determined. An ingenious variation in the application of the method was made by Pritulo[4] who demonstrated that if a perturbation solution in unstrained coordinates has been determined and found to be nonuniform, the coordinate straining required to render that solution uniformily valid can be found by employing straining directly in the known nonuniform solution, and then solving algebraic rather than differential equations. The idea of introducing strained coordinates a posteriori has since been applied to a variety of different problems (see ref. 3), and forms the basis of the current applications.

The fundamental idea underlying coordinate straining as it relates to the application of perturbation methods to supercritical transonic flows is illustrated geometrically in figure 1. In the upper plot on the left, two typical transonic pressure distributions are shown for a highly-supercritical flow about a nonlifting symmetric profile. The distributions can be regarded as related nonlinear flow solutions separated by a nominal change in some geometric or flow parameter. The shaded area between the solutions represents the perturbation result that would be obtained by directly differencing the two solutions. We observe that the perturbation so obtained is small everywhere except in the region between the two shock waves, where it is fully as large as the base solutions themselves. This clearly invalidates the perturbation technique in that region and most probably somewhat ahead and behind it as well. The key idea of a procedure for correcting this, pointed out by Nixon,[5,6] is first to strain the coordinates of one of the two solutions in such a fashion that the shock waves align, as shown in the upper plot on the right of figure 1, and then determine the unit perturbation. Equivalently, this can be considered as maintaining the shock wave location invariant during the perturbation process, and assures that the unit perturbation remains small both at and in the vicinity of the shock wave. Obviously, shock points are only one of a number of characteristic high-gradient locations such as stagnation points, maximum suction pressure points, etc., in which the accuracy of the perturbation solution can degrade rapidly. The plots in the lower left part of the figure 1 indicate such a situation and display typical transonic pressure distributions which contain multiple shocks and high-gradient regions. Simultaneously straining at all these locations, as indicated in the lower right plot, serves to minimize the unit perturbation over the entire domain considered, and provides the key to maximizing the range of validity of the perturbation method.

Theoretical Formulation

In order to provide the theoretical essentials of the correction method, consider the formulation of the procedure at the level of the full potential equation, as most of the results presented here are based on that level. We denote the operator L

acting on the velocity potential Φ as that which results in the two-dimensional full potential equation for Φ, i.e.

$$L[\Phi] = 0 \tag{2}$$

If we now expand the potential in terms of zero- and higher-order components in order to account for the variation of some arbitrary geometrical or flow parameter q

$$\begin{aligned} \Phi &= \Phi_0 + \varepsilon\Phi_1 + \ldots \\ q &= q_0 + \Delta q \end{aligned} \tag{3}$$

and then insert this into the governing equation (2), expand the result, order the equations into zero- and first-order components, and make the obvious choice of expansion parameter $\varepsilon = \Delta q$, we obtain the following governing equations for the zero- and first-order components

$$\begin{aligned} L[\Phi_0] &= 0 \\ L_1[\Phi_1] + \frac{\partial}{\partial q} L[\Phi_0] &= 0 \end{aligned} \tag{4}$$

Here L_1 is a linear operator whose coefficients depend on zero-order quantities and $\partial L[\Phi_0]/\partial q$ represents a 'forcing' term due to the perturbation. Actual forms of L_1 and the 'forcing' term are provided in reference 1 for a variety of flow and geometry parameter perturbations of a two-dimensional turbomachine, and in ref. 7 for profile shape perturbations of an isolated airfoil. An important point regarding equation (4) for the first-order perturbation Φ_1 is that the equation represents a unit perturbation independent of the actual value of the perturbation quantity ε.

Appropriate account of the movement of discontinuities and maxima of high-gradient regions due to the perturbation is now accomplished by the introduction of strained coordinates (s,t) in the form

$$\begin{aligned} x &= s + \varepsilon x_1(s,t) \\ y &= t + \varepsilon y_1(s,t) \end{aligned} \tag{5}$$

where

$$\begin{aligned} x_1(s,t) &= \sum_{i=1}^{N} \delta x_i x_{1_i}(s,t) \\ y_1(s,t) &= \sum_{i=1}^{N} \delta y_i y_{1_i}(s,t) \end{aligned} \tag{6}$$

and $\varepsilon\delta x_i$, $\varepsilon\delta y_i$ represents individual displacements of the N strained points, and $x_{1_i}(s,t)$, $y_{1_i}(s,t)$ are straining functions associated with each of the N strained points. Introducing the strained coordinate equations (5) and (6) into the expansion formulation leaves the zero-order result in equation (4) unchanged, but results in a change of the following form for the perturbation

$$L_1[\Phi_1] + L_2[\Phi_0] + \frac{\partial}{\partial q} L[\Phi_0] = 0 \tag{7}$$

Here the operators are understood to be expressed in terms of the strained (s,t) coordinates, and the additional operator L_2 arises specifically from displacement of the strained points. In references 6 and 7, specific expressions for L_2 are provided for selected perturbations involving transonic small-disturbance and full potential equation formulations. The primary point, however, with regard to perturbation equation (7) expressed in strained coordinates is that it remains valid as before for a unit perturbation and independent of ε.

In employing the correction method, equation (7), for the unit perturbation is solved by taking the difference between two solutions obtained by the full nonlinear procedure after appropriately straining the coordinates. If we designate the two solutions for some arbitrary flow quantity Q as base Q_0 and calibration Q_c, respectively, of the varied parameter, we have for the predicted flow at some new parameter value q (ref. 8)

$$Q(x,y) = Q_0(s,t) + \frac{\varepsilon}{\varepsilon_0}\left[Q_c(\bar{x},\bar{y}) - Q_0(s,t)\right] \tag{8}$$

where

$$\begin{aligned} \bar{x} &= s + \varepsilon_0 x_1(s,t) \\ \bar{y} &= t + \varepsilon_0 y_1(s,t) \\ x &= s + \frac{\varepsilon}{\varepsilon_0}[\bar{x} - s] \\ y &= t + \frac{\varepsilon}{\varepsilon_0}[\bar{y} - t] \\ \varepsilon_0 &= q_c - q_0 \\ \varepsilon &= q - q_0 \end{aligned} \tag{9}$$

Extension of this result to simultaneous multiple-parameter perturbations is straightforward (ref. 6); and that extension is provided in the following section where applications of the correction procedure are made to predict surface properties. Also provided are the particular forms of the straining functions equation (6) for those applications.

Current Applications: Surface Pressures

For the current applications, we have employed coordinate straining with the correction method to predict surface pressure distributions for a wide variety of single- and multiple-parameter geometrical and flow perturbations of isolated airfoils and cascades. In that instance where flow properties are required along some contour, the solutions can be represented by

$$\begin{aligned} Q(x;\varepsilon) &\sim Q_0(s) + \sum_{j=1}^{M} \varepsilon_j Q_{1_j}(s) + \ldots \\ x &\sim s + \sum_{j=1}^{M} \varepsilon_j x_1(s) + \ldots \end{aligned} \tag{10}$$

where x is the independent variable measuring distance along the contour or a convenient projection of that distance, s is the strained coordinate, and ε_j a small parameter representing the change in one of M flow or geometrical variables which we wish to vary simultaneously.

In order to determine the first-order corrections $Q_{1_j}(s)$, we require one base and M calibration

solutions in which the calibration solutions are determined by individually varying each of the M parameters by some nominal amount from the base flow value while keeping the others fixed at the base flow values.

In this way, the first-order corrections $Q_{1_j}(s)$ can be determined as

$$Q_{1_j}(s) = \frac{Q_{c_j}(\bar{x}_j) - Q_o(s)}{q_{c_j} - q_{o_j}} \tag{11}$$

where Q_{c_j} is the calibration solution corresponding to changing the jth parameter to a new value q_{c_j}, $\bar{x}_j$ is the strained coordinate pertaining to the Q_{c_j} calibration solution, and $q_{c_j} - q_{o_j}$ represents the change in the jth parameter from its base flow value. If we now desire to keep invariant during the perturbation process a total of N points corresponding to discontinuities or high-gradient maxima, we can represent the solution by:

$$Q(x_j;\varepsilon_j) = Q_o(s) + \sum_{j=1}^{M} \varepsilon_j Q_{1_j}(s) \tag{12}$$

where

$$Q_{1_j}(s) = \frac{Q_{c_j}(\bar{x}_j) - Q_o(s)}{\varepsilon_j^c} \tag{13}$$

$$\bar{x}_j = s + \sum_{i=1}^{N} \varepsilon_j^c (\delta x_i^c)_j x_{1_i}(s) \tag{14}$$

$$x = s + \sum_{j=1}^{M} \sum_{i=1}^{N} \varepsilon_j (\delta x_i)_j \, x_{1_i}(s) \tag{15}$$

$$\varepsilon_j^c = q_{c_j} - q_{o_j} \tag{16}$$

$$\varepsilon_j = q_j - q_{o_j} \tag{17}$$

$$\varepsilon_j^c (\delta x_i^c)_j = (x_i^c - x_i^o)_j \tag{18}$$

$$\varepsilon_j (\delta x_i^c)_j = \frac{\varepsilon_j}{\varepsilon_j^c} (x_i^c - x_i^o)_j \tag{19}$$

Here $\varepsilon_j^c(\delta x_i^c)_j$ given in equation (18) represents the displacement of the ith invariant point in the jth calibration solution from its base flow location due to the selected change ε_j^c in the q_j parameter given by equation (16), $\varepsilon_j(\delta x_i^c)_j$ given in equation (19) represents the predicted displacement of the ith invariant point from its base flow location due to the desired change ε_j in the q_j parameter given by equation (17), and $x_{1_i}(s)$ is a unit-order straining function having the property that

$$x_{1_i}(x_k^o) = \begin{cases} 1 & k = i \\ 0 & k \neq i \end{cases} \tag{20}$$

which assures alignment of the ith invariant point between the base and calibration solutions.

In addition to the single condition equation (20) on the straining function, it may be convenient or necessary to impose additional conditions at other locations along the contour. For example, it is usually necessary to hold invariant the end points along the contour, as well as to require that the straining vanish in a particular fashion in those locations. All of these conditions, however, do not serve to determine the straining uniquely. The nonuniqueness of the straining, nevertheless, can often be turned to advantage, either by selecting particularly simple classes of straining functions or by requiring the straining to satisfy further constraints convenient for a particular application. An example of the effect of employing two different straining functions for a strongly-supercritical flow was provided in reference 6. Here we provide additional results demonstrating some of the limitations of various polynomial straining functions and provide some comparisons with piecewise-continuous functions. The particular classes of straining functions employed were continuous polynomial and linear piecewise-continuous. For these two classes, the functional forms of the straining can be compactly written. For example, equation (14) becomes, for continuous polynomial straining

$$\bar{x}_j = s + \sum_{i=2}^{N-1} L_i(s) \cdot (x_i^c - x_i^o) \tag{21}$$

where L_i are Lagrangian coefficients given by

$$L_i(s) = \prod_{\substack{k=1 \\ k \neq i}}^{N} \frac{(s - x_k^o)}{(x_i^o - x_k^o)} \tag{22}$$

where as for linear piecewise-continuous straining, $\bar{x}_j$ is given by

$$\bar{x}_j = s + \sum_{i=2}^{N-1} \left\{ \frac{x_{i+1}^o - s}{x_{i+1}^o - x_i^o} \cdot (x_i^c - x_i^o) + \frac{s - x_i^o}{x_{i+1}^o - x_i^o} \cdot (x_{i+1}^c - x_{i+1}^o) \right\} H(x_{i+1}^o - s) \times H(s - x_i^o) \tag{23}$$

where H denotes the Heaviside step function. As discussed above, it is usually necessary to hold invariant both of the end points along the contour in addition to the points corresponding to discontinuities or high-gradient maxima. Consequently, for the results reported here, the array of invariant points in the base and calibration solutions have been taken as

$$x_i^o = \{0, x_1^o, x_2^o, \ldots, x_n^o, 1\}$$
$$x_i^c = \{0, x_1^c, x_2^c, \ldots, x_n^c, 1\} \tag{24}$$

where the contour length has been normalized to one. Figure 2 provides a summary of the various combinations of flows and straining functions employed.

Results

One of the primary objectives of the present investigation is to explore the accuracy and range of validity of such perturbation procedures to determine to what extent they are capable of providing results useful in an engineering analysis. To this end, we have tested the correction method with coordinate straining over a variety of different geometrical and flow condition perturbations, including applications to both isolated airfoils and compressor cascades. In particular, since the ability of the method to account accurately for the movement of discontinuities and maxima of high-gradient but continuous regions is essential if such procedures are to be of general use, emphasis was placed on transonic flows which are strongly supercritical and exhibit large surface shock movement over the parametric range studied. Base flow theoretical solutions were determined from small-disturbance transonic potential[9] and full potential solutions[10,11,12]. In the results to follow, which were selected as typical from systematic calculations of a much larger number of cases, the choice of base and calibration solutions was often made at the limits of validity of the procedure to observe how well the method works under such conditions.

Single-Parameter Perturbations

Supercritical applications. In figure 3, we present results for a thickness-ratio perturbation of strongly-supercritical flows past a nonlifting cascade of biconvex profiles at $M_\infty = 0.80$ having a spacing-to-chord ratio of $H/C = 1.0$. The dotted and dashed results on the figure represent the base and calibration surface pressure distributions for $\tau = (0.075, 0.065)$, respectively, and were obtained by solving the transonic small-disturbance potential equation using the code TSFOIL[9]. An x-grid having 48 points on the blade profile was used. These solutions, then, were used to determine the unit perturbation. The open circles represent the perturbation solution for $\tau = 0.073$ in the plot on the left and for $\tau = 0.070$ in the plot on the right. Those perturbation results are meant to be compared with the solid lines in the plots which are the corresponding nonlinear solutions obtained by rerunning TSFOIL at the new thickness ratios. Quadratic straining was used with shock point and leading and trailing edges held invariant. The base and calibration flow shock-point locations for this example, as well as for all of the supercritical cases presented here, were determined as the point where the pressure coefficient passed through critical with compressive gradient.

With regard to the results, several points are noteworthy. Selection of a cascade rather than an isolated airfoil provides a more sensitive transonic flow situation. Additionally, the choice of a highly-supercritical base and almost-subcritical calibration solution provides both an example of extreme separation between the two nonlinear solutions used to define the unit perturbation, as well as a situation where one solution is near the limits of validity of the perturbation analysis. Recall that both solutions must be topographically similar, i.e., must contain the same number of discontinuities (shocks) and other characteristic features.

We note that comparisons of the perturbation results with the nonlinear calculations are very satisfactory for both thickness ratios, with the only discrepancy being a slight disagreement at the lower thickness ratio ($\tau = 0.070$) at several points in the post-shock region. Additional calculations not presented here in which a more reasonable choice of calibration solution is made, say at $\tau = 0.070$, removes that discrepancy as well. The main point provided by the results of figure 3 is that for certain classes of supercritical flows even widely-separated base solutions can be used to provide reasonable perturbation predictions.

In figure 4, we provide similar strongly-supercritical results again for interpolation-only perturbation solutions, but in this instance on a somewhat finer grid. These results employed full potential base solutions[10], and represent thickness ratio perturbations of nonlifting symmetric free-air flows past NACA four-digit thickness-only airfoils at $M_\infty = 0.820$. The body-fitted mesh employed had 75 points on both upper and lower surfaces, which is half-again as many as in the preceding example. For the base and calibration flows, the thickness ratios were $\tau = 0.120$ and 0.080, respectively. Comparisons between the perturbation predictions and the full nonlinear calculation are exhibited in figure 4 for $\tau = 0.110$, 0.105, 0.100, and 0.095. We note that the comparisons are remarkably good, in particular, in the region of the shock. The first-order perturbation accurately predicts both shock location and the post-shock expansion behavior. Reference to the coarser grid results given in figure 3 indicates that the finer grid resolution clearly enhances the perturbation result, indicating that better accuracy and a larger range of validity of the perturbation solutions can be anticipated when fine-grid base solutions are used to define the unit perturbation.

In the two preceding examples, perturbation results were provided for interpolation-only between widely-spaced base and calibration solutions. In figure 5, we provide similar strongly-supercritical thickness-ratio perturbation results for extreme solution extrapolation using very closely-spaced base and calibration solutions[10]. The upper plots display results for extrapolation downward from base and calibration flows past nonlifting NACA OOXX profiles with $\tau = 0.115$ and 0.120 at $M_\infty = 0.820$. Perturbation predictions are shown for $\tau = 0.105$ and 0.100, which represent $\Delta\tau$ excursions from the base flow ($\tau = 0.115$) that are two and three times the parameter change between the base and calibration solutions ($\Delta\tau = 0.005$) used to define the unit perturbation. For these results, comparisons with the full nonlinear calculations are very good. The lower plots display similar results for extreme extrapolation upward from base and calibration solutions having $\tau = 0.095$ and 0.090. Perturbation predictions are shown for $\tau = 0.105$ and 0.110, which again represent excursions from the base flow that are two and three times the parameter change between the base and calibration solutions. In this instance, while comparisons of the perturbation results and the full nonlinear solutions for both cases are good, the results at $\tau = 0.110$ are beginning to display some not-surprising discrepancies near the shock wave, indicating that the perturbation result is nearing the limit of its range of validity for this particular choice of base and calibration flows.

The results indicated in figure 5, however, clearly demonstrate that not only is accurate solution extrapolation possible, but that for some situations even closely-spaced nonlinear solutions can be used to cover a wide range of related solutions. Additionally, the range of parameter variation in this example over which the perturbation results remain accurate - i.e., parameter changes three times the difference between the two nonlinear solutions used to define the unit perturbation - is remarkable, and far beyond what one would anticipate for a first-order correction.

Perturbation results using a more reasonable choice of base and calibration solutions are provided in figure 6. Those results involve Mach number perturbations of highly-supercritical full potential[10] flows past a NACA 0012 airfoil at $\alpha = 0°$. The base and calibration results are for $M_\infty = 0.800$ and 0.820, and the comparisons indicated are for perturbation results interpolated to $M_\infty = 0.810$ and extrapolated downward to $M_\infty = 0.790$. As in the case of the geometric perturbations given in figures 4 and 5, these perturbation results are also in very good agreement with the nonlinear calculations at the new Mach numbers. For this perturbation, as well as for a number of other Mach number perturbations, we have separately determined the perturbation result in two different ways. First, we have taken cognizance of the fact that a Mach number perturbation alters the governing differential equation for the first-order perturbation from that of other geometric or flow parameter changes; and have used the suggestion of reference 6 to consider such perturbations via a transonic small-disturbance approximation, whereby the same perturbation equation can be preserved by employing a modified expansion parameter ε. An alternative procedure is to treat a Mach perturbation directly and interpret ε as the difference in Mach number. We have done these calculations and compared the perturbation results for a number of cases using both full potential solutions, as for the results shown in figure 6, and transonic small-disturbance solutions, and have observed no essential difference between the two sets of results. The perturbation results presented in figure 6 correspond to those for ε equal to the difference in Mach number.

All of the supercritical perturbation results presented in figures 3 to 6 have been for symmetric flows and have employed a quadratic straining function. In figure 7, we present results for an angle of attack perturbation of lifting flows past a NACA 0012 profile at $M_\infty = 0.70$. The full potential[10] base and calibration solutions are at $\alpha = 3.0°$ and 4.0°, with comparisons of the perturbation and full nonlinear results shown for $\alpha = 3.5°$ and 2.5°. Cubic straining has been used with the invariant points corresponding to the lower trailing edge, stagnation point, shock point, and the upper trailing edge (see Fig. 2). We note that at $\alpha = 3.5°$, the perturbation results are very good everywhere, in particular, in the vicinity of the shock and stagnation regions. At $\alpha = 2.5°$, the perturbation results are still very good in the shock and stagnation regions and on most of the upper and lower surface, but near the trailing edge of a discrepancy has occurred. The cause of this discrepancy lies solely with the straining function (cubic) used. It is due to the fact that although the straining vanishes identically at the trailing edge, for the particular choice of base and calibration solutions in this example, the straining in the near vicinity of the trailing edge becomes sufficiently large to introduce a misalignment in the unit perturbation in that high-gradient region. The correction to this is discussed in the section describing piecewise-continuous straining functions.

Subcritical applications. Although supercritical flows are clearly of central concern in any transonic analysis for which the perturbation methods presented here would be used, applications to subcritical nonlinear flows are also of significance. To this end, we have applied these same techniques to a variety of subcritical flows to examine their accuracy and range of validity for such applications.

In figure 8, we present some summary results for four different subcritical perturbation applications to an isolated airfoil. All of these results are based on full potential solutions[10] with quadratic straining holding invariant the stagnation point and the trailing edge points. The plot on the upper left displays comparisons for a camber line perturbation of a lifting flow with $M_\infty = 0.50$ and $\alpha = 2°$ past an airfoil having a NACA 0012 thickness distribution and a parabolic-arc camber line having the maximum camber located at midchord. Base and calibration flows with camber ratio $h/c = 0.02$ and 0.01 were used to extrapolate perturbation results to $h/c = 0.05$. Comparisons with full result is essentially exact. The plot on the upper right provides similar results for a thickness-ratio perturbation of a lifting flow with $M_\infty = 0.50$ and $\alpha = 2°$ past NACA 00XX thickness-only airfoils. Base and calibration flows with $\tau = 0.12$ and 0.04 were used to provide interpolation results at $\alpha = 0.08$. Again, the agreement is essentially exact even in the peak suction pressure region. The plot on the lower left provides angle-of-attack perturbation results for $M_\infty = 0.50$ flow past a NACA 0012 airfoil, using base/calibration results for $\alpha = 4.0°$, 2.0° to predict results at $\alpha = 3.0°$, with the agreement again being quite good. The final comparisons given in the plot on the lower left are for a Mach number perturbation of a lifting flow at $\alpha = 2°$ past an airfoil having a NACA 0012 thickness distribution and a parabolic-arc camber line with camber ratio $h/c = 0.03$ at midchord. Base/calibration results at $M_\infty = 0.40$, 0.60 were used to predict results at $M_\infty = 0.55$, with good agreement with the full nonlinear calculation.

In figure 9, we present similar summary results for subcritical perturbation applications to a compressor cascade having a 4% biconvex thickness distribution and a 1% parabolic-arc camber line blade, a pitch of $t/c = 0.37$, and oncoming Mach number $M_\infty = 0.770$. These results are based on the full potential solution procedure of reference 11 and have also used quadratic straining to hold the trailing edge points and stagnation point invariant. The plots in the upper part of the figure represent an inflow angle perturbation, with base/calibration inflow angles $\beta_i = 47.8°$, 49.8° used to predict extrapolation results in the plot on the left for $\beta_i = 44.8°$ and interpolation results in the plot on the right for $\beta_i = 48.8°$. In the lower left plot, interpolation results are displayed for an outflow angle perturbation with base/calibration outflow

angles β_0 = 31.5°, 39.5° used to predict the flow at β_0 = 35.5°. The lower right plot provides interpolation results for a rotational speed perturbation with base/calibration rotational speeds ω = 967, 667 rad/sec used to predict the flow at ω = 827 rad/sec. In all of these results, the perturbation results are good, including the regions near the leading and trailing edge where a peaky behavior due to local grid resolution is observed.

Piecewise-Continuous Straining Functions

The results presented in figures 10 to 13 illustrate the effect of using different straining functions to determine the perturbation results. Comparisons are provided for several strongly-supercritical flows, demonstrating the differences in perturbation solutions between using quadratic and cubic straining functions and corresponding piecewise-continuous straining functions.

Figure 10 displays a comparison for a symmetric supercritical thickness-ratio perturbation at τ = 0.110 for which results based on quadratic straining were given in figure 4. In that figure, the open circles denote the previously-obtained perturbation result using quadratic straining, while the asterisks denote the corresponding result when using linear piecewise-continuous straining. The points held invariant are the leading and trailing edges and the shock point. For this case there is virtually exact agreement everywhere between the two perturbation results as well as with the nonlinear result. An analogous comparison with a cubic straining result is provided in figure 11 where the invariant points are the lower trailing edge, stagnation point, shock point, and upper trailing edge. Displayed in that figure as open circles are the cubic-straining supercritical angle-of-attack perturbation results at α = 2.5° which were previously given in figure 7. Asterisks denote the corresponding linear piecewise-continuous straining perturbation result. We note that the discrepancy near the trailing edge caused by the cubic straining has been effectively removed in the piecewise-continuous result. Moreover, the good agreement with the full nonlinear result which the cubic result displayed near the shock and stagnation regions, as well as over the remainder of the airfoil surface, is also obtained with the piecewise-continuous result.

Finally, we have found that when employing quadratic, cubic, and higher-order polynomials as straining functions, for certain combinations of base flow shock location and shock movement between base and calibration solutions, particularly when large shock movements are involved, the polynomial straining functions will strain some points off the airfoil surface. This of course, invalidates the determination of the unit perturbation, and requires that a different straining function be employed. Piecewise-continuous straining functions provide a simple means of avoiding such difficulties.

In figures 12 and 13, we have provided examples illustrating this effect for both quadratic and cubic straining functions. Figure 12 provides a comparison of perturbation results obtained using quadratic (open circles) and linear piecewise-continuous (asterisks) straining applied to a supercritical Mach number perturbation for symmetric nonlifting flow past a NACA 0012 airfoil. Widely-separated base/calibration flows[10] at M_∞ = 0.820 and 0.750 were used to predict the flow at M_∞ = 0.810. The spurious behavior near the leading edge displayed by the open circles is due to the quadratic function moving points in the strained calibration solution off the airfoil surface. The piecewise-continuous results indicated by the asterisks display a smooth variation in that region, and provide good agreement everywhere with the full nonlinear result. Figure 13 provides a corresponding comparison for cubic straining. Angle-of-attack perturbation results at M_∞ = 0.70 for flow past a NACA 0012 profile using base/calibration results[10] at α = 2.25° and 4.00° are used to predict the flow at α = 3.25°. The unusual results displayed by the open symbols near the trailing edge indicate that the cubic function has strained points off the airfoil surface in that region. However, the linear piecewise-continuous result corrects that problem and displays good agreement with the nonlinear calculation in that region as well as at the shock and stagnation point.

Multiple-Parameter Perturbations

All of the previous results presented in figures 3 to 13 were for single-parameter perturbations of some flow or geometry parameter. In figures 14 to 16, we provide corresponding results for the simultaneous perturbation of two or more parameters of strongly-supercritical transonic flows. In figure 14, comparisons are provided for the simultaneous perturbation of thickness-ratio and oncoming Mach number of highly-supercritical full potential[10] flows past NACA four-digit airfoils. The base flow chosen is at M_∞ = 0.820 and τ_B = 0.120, and is indicated in both plots in figure 14 as the dashed line. The calibration flow selected to account for Mach number changes is at M_∞ = 0.800 and τ = 0.120, and is displayed as the dotted line in the plot on the left; while the calibration flow selected to account for thickness-ratio changes is at M_∞ = 0.820 and τ = 0.110 and is displayed in the plot on the right. The comparisons between the perturbation and exact nonlinear results are for parameter extrapolation to M_∞ = 0.790 and τ = 0.115. We note that the indicated results for base, perturbation, and exact nonlinear solution in both plots of figure 14 are the same; the primary reason for presenting two plots is to indicate clearly the separation between the base, the two calibration solutions, and the predicted result. The straining employed is linear piecewise-continuous, with leading and trailing edge and shock point held invariant. With regard to the results, the comparison between the perturbation and the exact nonlinear result is, as in the case of single-parameter perturbations of these flows (Figs. 4 to 6), extremely good, in particular in the region of the shock. We note that the particular parameter values of (M_∞,τ) = (0.790, 0.115) selected for the prediction solution represent reasonably substantial extrapolations from the base and calibration values. Nevertheless, the perturbation method is able to treat this large extrapolation range accurately.

Figure 15 presents analogous three-parameter perturbation results when angle-of-attack variations are included for the flows shown in figure 14.

Here, the base flow selected is at $\alpha = 0.2°$, $M_\infty = 0.800$, $\tau = 0.110$, and is indicated in all of the three plots provided as the dashed line. The calibration flow to account for angle-of-attack change is at $\alpha = 0.25°$ at the same (M_∞,τ) as the base flow, and is displayed as the dotted curve in the plot on the upper left. The corresponding calibration flow to account for Mach number change is at $M_\infty = 0.810$ and is displayed in the upper right plot, while the calibration flow for thickness-ratio change is at $\tau = 0.115$, and shown in the lower plot. The predicted result is for parameter values of $\alpha = 0.3°$, $M_\infty = 0.820$, $\tau = 0.100$ and again represents reasonably substantial extrapolations of all three parameters, as can be observed in figure 15 from the relative differences between the base and calibration flows. The reason for selecting such small angles-of-attack for these flows was to preserve the shock wave on the lower surface, and thereby create a set of multiple-shock flows which were highly sensitive to parameter changes. The comparisons between perturbation and exact nonlinear results for this case is again extremely good, with the prediction of both the locations of the shocks on the upper and lower surface given very well, as well as the pressure distributions in the regions immediately ahead and behind those shocks. For these results, linear piecewise-continuous straining was employed with the invariant points being the lower surface trailing edge, lower surface shock, stagnation point, upper surface shock, and upper surface trailing edge. The final result provided in figure 16 is for a four-parameter perturbation of strongly-supercritical full potential[12] flows past a cascade of blades having NACA four-digit profiles. The base flow is for an oncoming Mach number of $M_\infty = 0.780$, thickness-ratio $\tau = 0.110$, gap-to-chord ratio $t = 3.2$, and oncoming inflow angle $\alpha = 0.3°$. The four calibration solutions to account for changes in these parameters are provided in the four plots shown where the individual values of the calibration parameter varied are also indicated. The comparison of the predicted and exact nonlinear results are for parameter values of $M_\infty = 0.785$, $\tau = 0.115$, $t = 3.1$, $\alpha = 0.5°$. This particular set of flows was again selected because of the presence of multiple-shocks and high sensitivity to parameter change. We note that the perturbation predictions are once more remarkably accurate.

Nonphysical Applications

The results provided in figures 3 to 16 have been exclusively for perturbations of parameters which are physical in origin, i.e. either geometrical or flow quantities. However, many perturbation problems arise from nonphysical bases. An example which is important for the present applications is the difference between solutions representing different levels of approximation to the same problem. In this sense, finite difference solutions obtained on a coarse mesh should be correctable, employing ideas of the perturbation method discussed, to provide a fine mesh result. Similarly, various levels of approximation of the governing equations for the same problem lead to differences in solutions that can be regarded in an analogous fashion. Thus, the differences between transonic small-disturbance, full potential, Euler, and Navier-Stokes equation solutions can be viewed in the present context as various perturbation problems. Results for grid corrections and level-of-equation approximations have been successfully carried out and are reported in reference 8. All of these results, taken in toto, serve to demonstrate both the power and versatility of perturbation methods based on such ideas.

Concluding Remarks

An evaluation has been made of a perturbation procedure for determining highly-accurate approximations to families of nonlinear solutions which are either continuous or discontinuous, and which represent variations in some arbitrary parameter. The procedure employs unit perturbations, determined from two or more nonlinear solutions which differ from one another by a nominal change in some geometric or flow parameter, to predict a family of related nonlinear solutions. Coordinate straining is used in determining the unit perturbation in order to account properly for the motion of discontinuities and maxima of high-gradient regions. Extensive perturbation calculations based on full potential nonlinear solutions have been carried out. These calculations cover a variety of flow and geometric parameter perturbations involving isolated airfoils and compressor cascades at both subsonic and transonic flow conditions. Particular emphasis was placed on supercritical transonic flows which exhibit large surface shock movements over the parameter range studied; and on subsonic flows which display large pressure variations in the stagnation and peak suction pressure regions. Perturbation results, for both single- and multiple-parameter perturbations, characterized by both extreme solution interpolation using widely-separated base flow solutions and extreme solution extrapolation using closely-spaced base flow solutions, were obtained in order to determine the accuracy and range of validity of the method. Additionally, calculation of perturbation results were made to investigate the effectiveness of employing piecewise-continuous straining functions rather than polynomial (quadratic, cubic, quartic) functions.

Comparisons of the perturbation results with the corresponding 'exact' nonlinear solutions indicate a remarkable accuracy and range of validity of the perturbation method across the spectrum of examples reported. Solution interpolation and extrapolation are both feasible. Results evaluating the polynomial and piece-wise-continuous straining functions indicate that the piecewise-continuous functions are superior. Computational time of the method, beyond the determination of the base solutions, is trivial. Based on these results, we conclude that such a perturbation procedure can provide a means for substantially reducing computational requirements in design studies or other applications where large numbers of related nonlinear solutions are needed.

Acknowledgments

The results reported are based on research supported by NASA/Lewis Research Center under Contract NAS3-20836 with Dr. William D. McNally as Technical Monitor. Special thanks are due to Dr. Terry L. Holst of NASA/Ames Research Center for making available the isolated airfoil full potential solver[10], and to Dr. Djordje S. Dulikravich for the cascade full potential solver[12].

References

1. Stahara, S. S., Chaussee, D. S., and Spreiter, J. R.: Perturbation Solutions for Transonic Flow on the Blade-to-Blade Surface of Compressor Blade Rows. NASA CR-2941, Jan. 1978.

2. Lighthill, M. J.: A Technique for Rendering Approximate Solutions to Physical Problems Uniformly Valid. Philos. Mag., Vol. 40, 1949, pp. 1179-1201.

3. Van Dyke, M.: Perturbation Methods in Fluid Mechanics. The Parabolic Press, California, 1975.

4. Pritulo, M. F.: On the Determination of Uniformly Accurate Solutions of Differential Equations by the Method of Perturbation of Coordinates. J. Appl. Math. Mech., Vol. 26, 1962, pp. 661-667.

5. Nixon, D.: Perturbation of a Discontinuous Transonic Flow. AIAA J., Vol. 16, Jan. 1978, pp. 47-52.

6. Nixon, D.: Perturbations in Two- and Three-Dimensional Transonic Flows. AIAA J., Vol. 16, July 1978, pp. 699-709.

7. Nixon, D.: Design of Transonic Airfoil Sections Using a Similarity Theory. NASA TN 7851, Oct. 1978.

8. Nixon, D.: Perturbation Methods in Transonic Flow. AIAA Paper No. 80-1367, July 1980.

9. Stahara, S. S.: Operational Manual for Two-Dimensional Transonic Code TSFOIL. NASA CR-3064, Dec. 1978.

10. Holst, T. L. and Ballhaus, W. F.: Fast, Conservative Schemes for the Full Potential Equation Applied to Transonic Flows. AIAA J., Vol. 17, Feb. 1979, pp. 145-152.

11. Katsanis, T.: Fortran Program for Calculating Transonic Velocities on a Blade-to-Blade Stream Surface of a Turbomachine. NASA TN D-5427, Sept. 1969.

12. Kulikravich, D. S.: CAS2D: Computer Program for Planar Steady Potential Cascade Flows. To be published as a NASA TP.

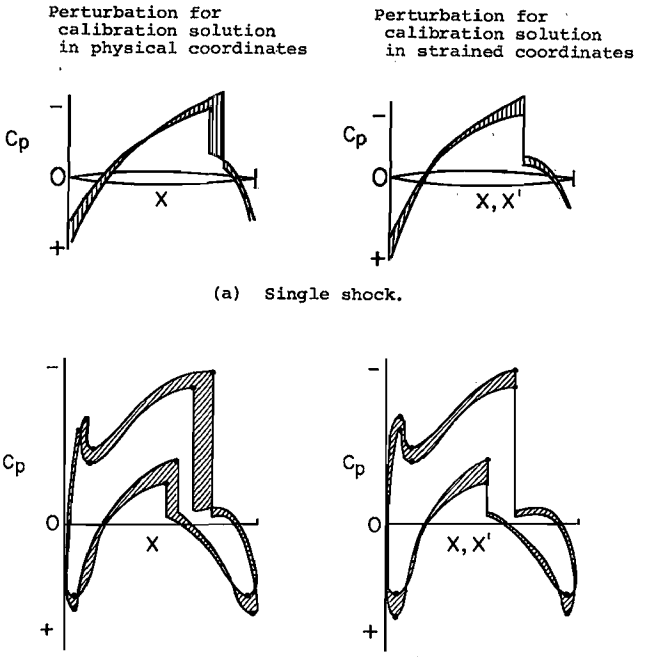

Fig. 1 Illustration of perturbation solution for calibration solution in physical and strained coordinates

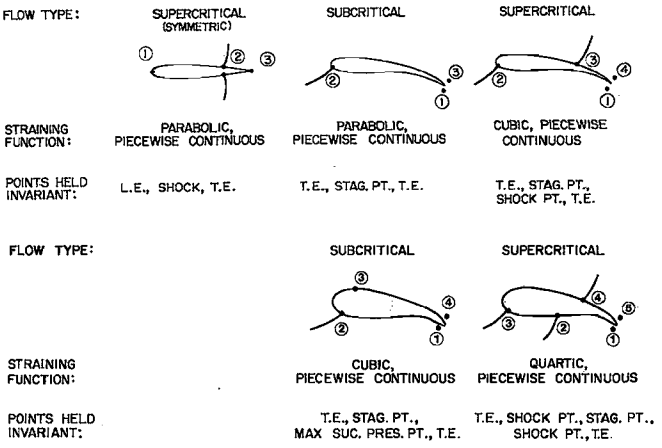

Fig. 2 Summary of various flows and straining functions considered

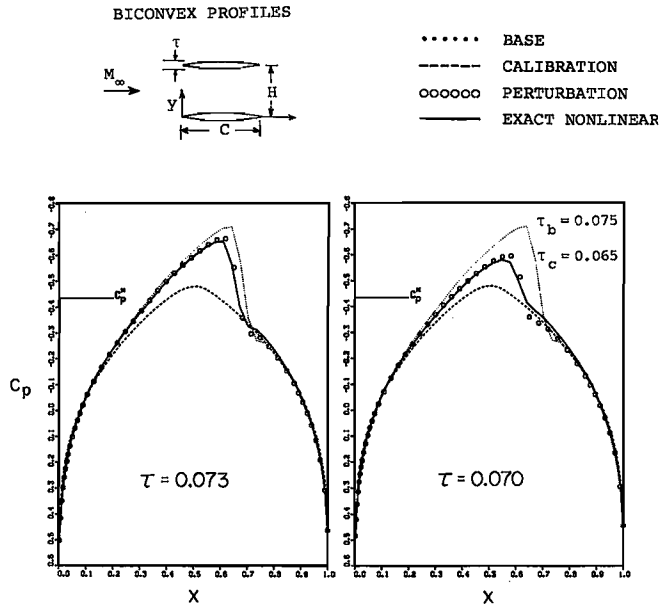

Fig. 3 Comparison of perturbation (O) and nonlinear (—) surface pressures for a thickness-ratio perturbation of a nonlifting cascade of biconvex profiles with H/C = 1.0 at $M_\infty = 0.80$

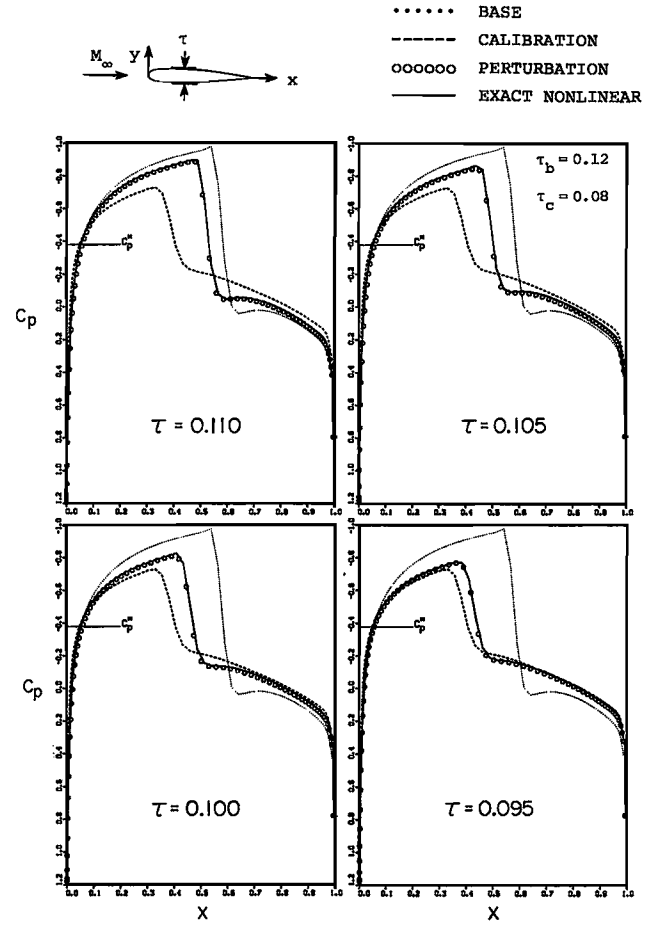

Fig. 4 Comparison of perturbation (O) and nonlinear (—) surface pressures for a thickness-ratio perturbation for an isolated NACA 00XX airfoil at $M_\infty = 0.820$ and $\alpha = 0°$ for solution interpolation

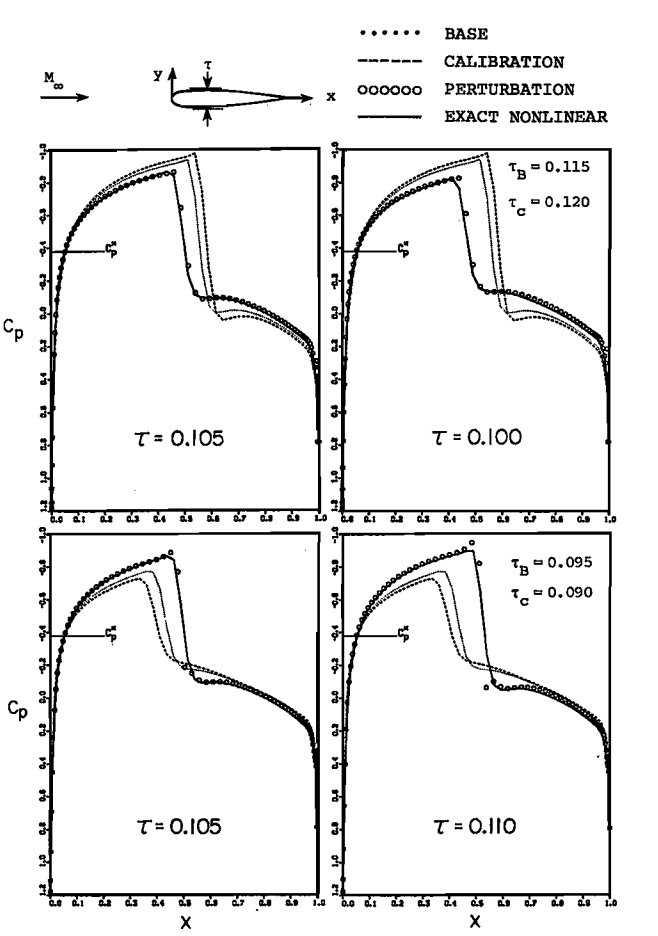

Fig. 5 Comparison of perturbation (O) and nonlinear (—) surface pressures for a thickness-ratio perturbation for an isolated NACA 00XX airfoil at $M_\infty = 0.820$ and $\alpha = 0°$ for extreme solution extrapolation

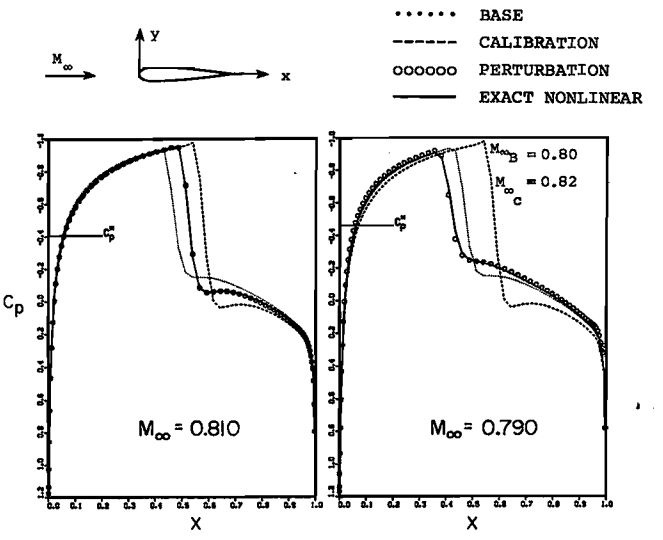

Fig. 6 Comparison of perturbation (O) and nonlinear (—) surface pressures for a Mach number perturbation of an isolated NACA 0012 airfoil at $\alpha = 0°$

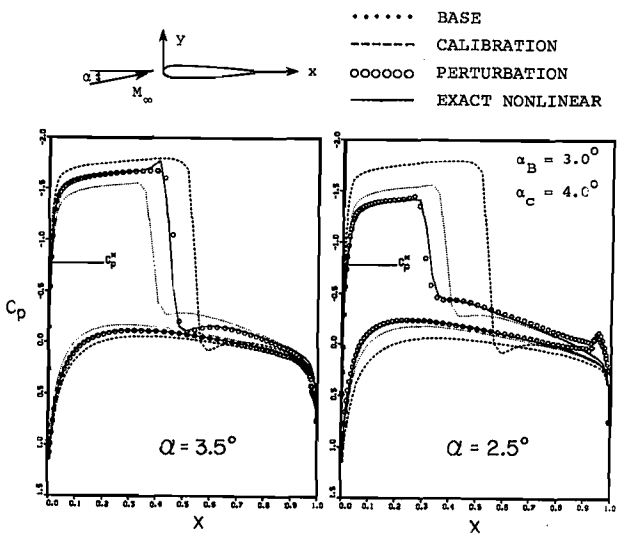

Fig. 7 Comparison of perturbation (o) and nonlinear (—) surface pressures for an angle-of-attack perturbation of an isolated NACA 0012 airfoil at $M_\infty = 0.70$

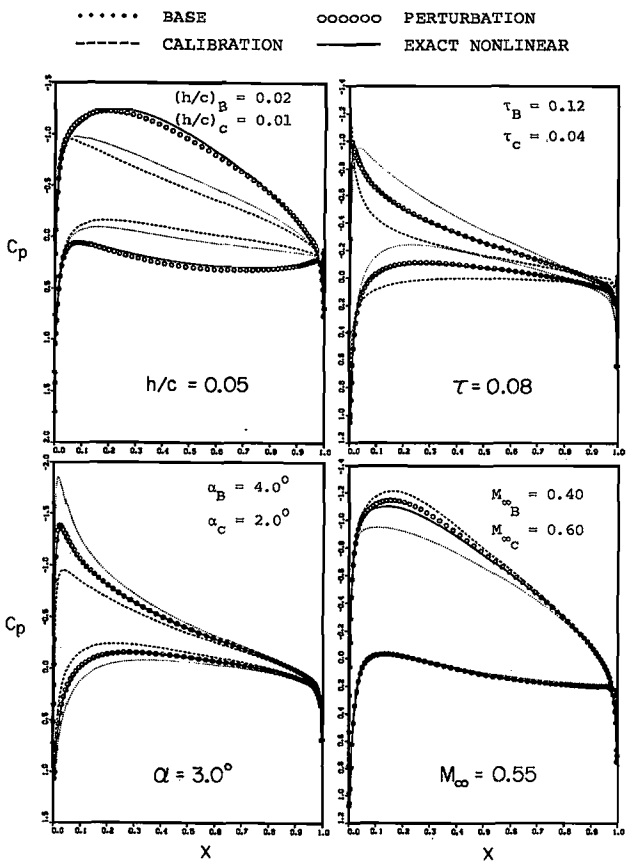

Fig. 8 Comparison of perturbation (o) and nonlinear (—) surface pressures for various geometry and flow parameter perturbations of isolated airfoils at subcritical speeds

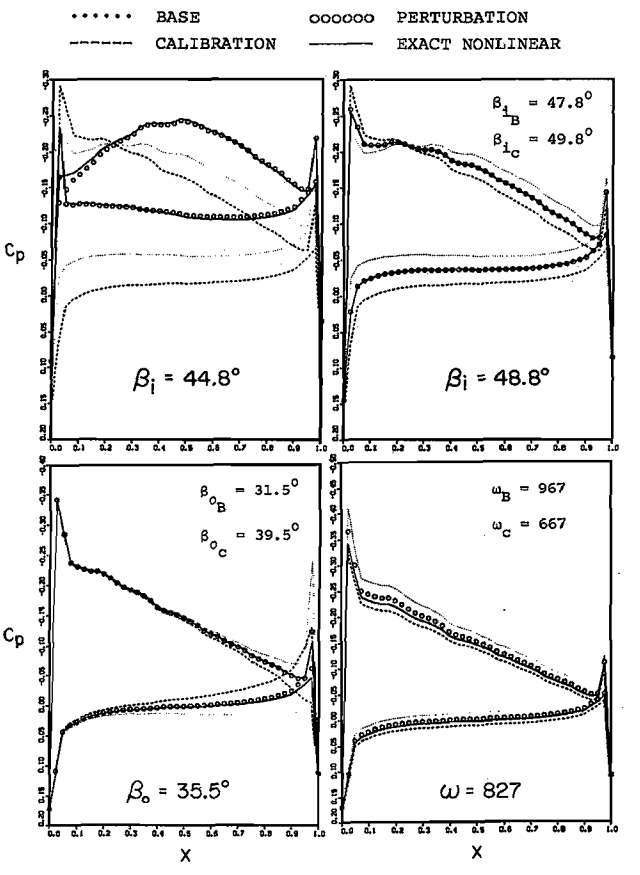

Fig. 9 Comparison of perturbation (o) and nonlinear (—) surface pressures for various flow parameter perturbations of a compressor cascade at subcritical speeds

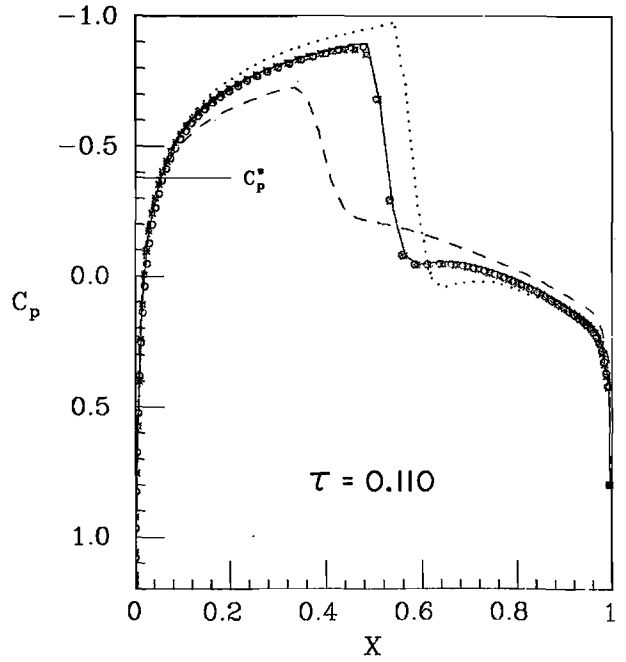

Fig. 10 Comparison of nonlinear (—) surface pressures with perturbation results using quadratic (O) and linear piecewise-continuous (*) straining functions for a thickness-ratio perturbation of an isolated NACA 00XX airfoil at $M_\infty = 0.820$ and $\alpha = 0°$

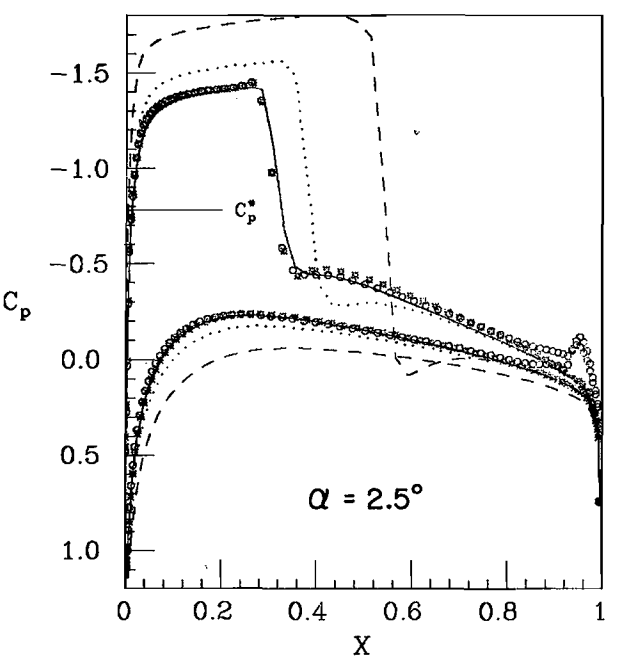

Fig. 11 Comparison of nonlinear (—) surface pressures with perturbation results using cubic (O) and linear piecewise-continuous (*) straining functions for an angle-of-attack perturbation of an isolated NACA 0012 airfoil at $M_\infty = 0.70$

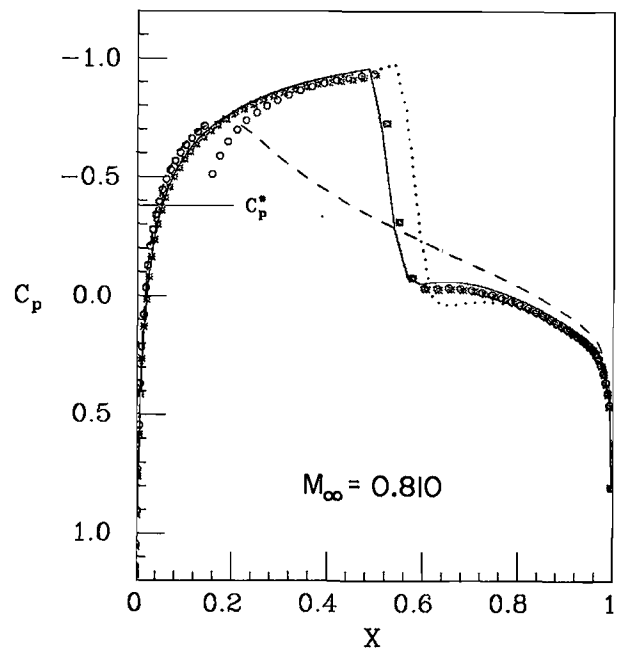

Fig. 12 Comparison of nonlinear (—) surface pressures with perturbation results using quadratic (O) and linear piecewise-continuous (*) straining functions for a Mach number perturbation of an isolated NACA 0012 airfoil at $\alpha = 0°$

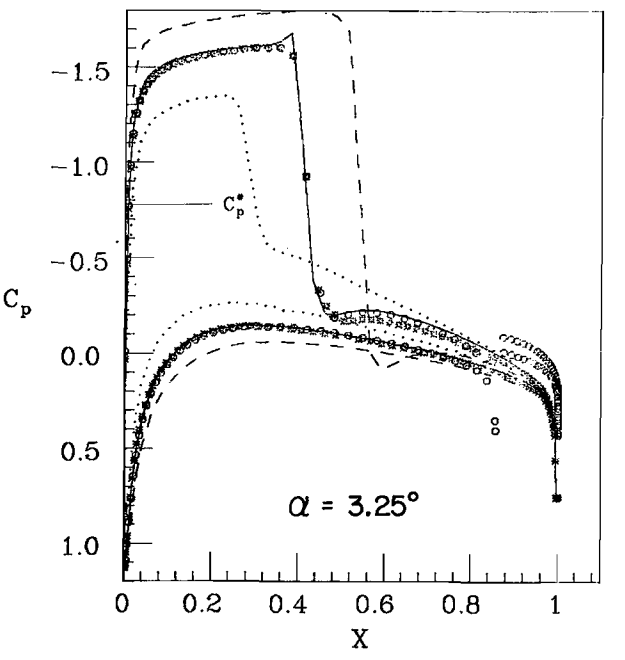

Fig. 13 Comparison of nonlinear (—) surface pressures with perturbation results using cubic (O) and linear piecewise-continuous (*) straining functions for an angle-of-attack perturbation of an isolated NACA 0012 airfoil at $M_\infty = 0.70$

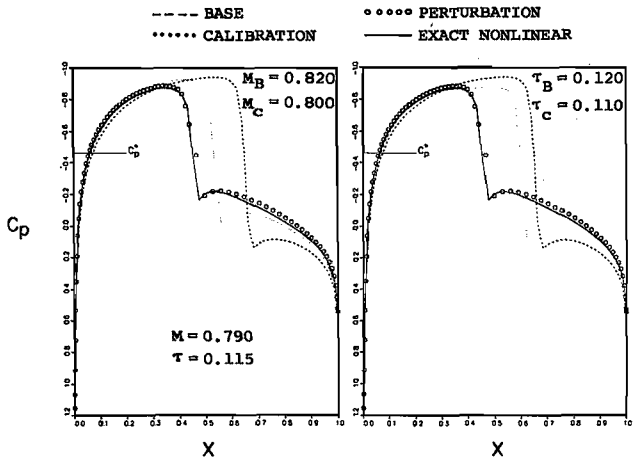

Fig. 14 Comparison of perturbation (O) and nonlinear (—) surface pressures for simultaneous Mach number and thickness-ratio perturbation of a nonlifting isolated NACA 00XX airfoil

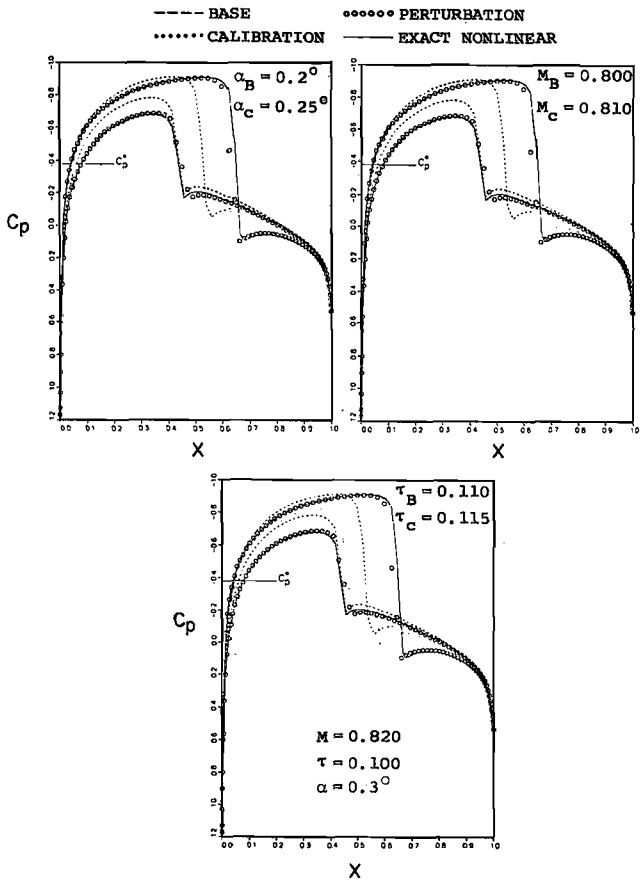

Fig. 15 Comparison of perturbation (O) and nonlinear (—) surface pressures for simultaneous angle-of-attack, Mach number, and thickness-ratio perturbation of a isolated NACA 00XX airfoil

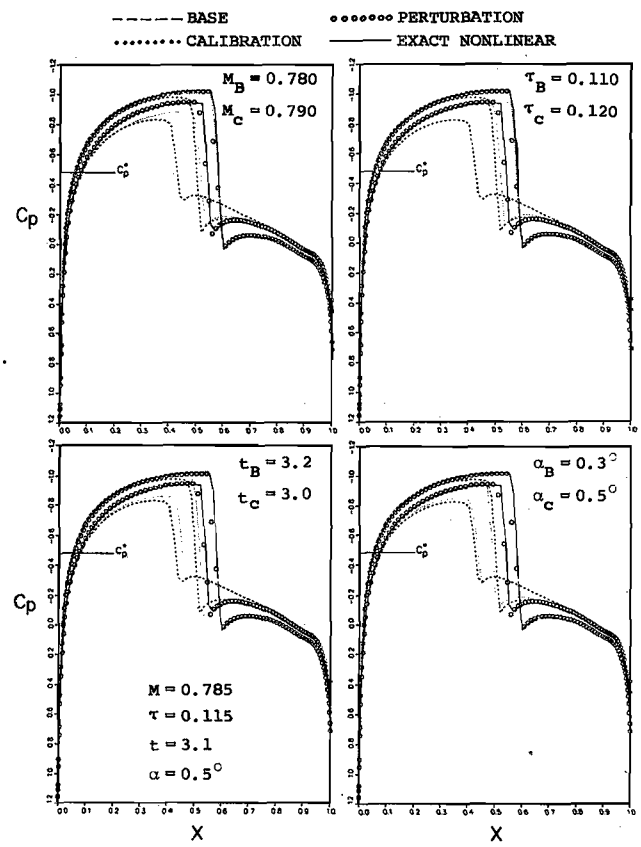

Fig. 16 Comparison of perturbation (O) and nonlinear (—) surface pressures for simultaneous Mach number, thickness-ratio, spacing ratio, and oncoming flow angle perturbation of a cascade of NACA 00XX blades